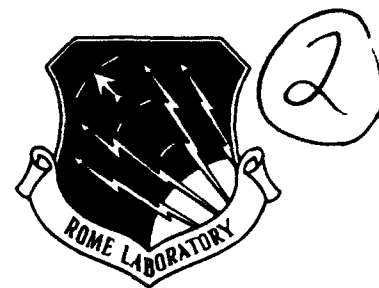


**AD-A276 722**



**RL-TR-93-248**  
**Final Technical Report**  
**December 1993**



# **DEVELOPMENT OF PHASE- ONLY FILTERS FOR SENSOR IMAGERY**

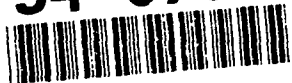
**Florida Institute of Technology**

**Samuel P. Kozaitis**

**DTIC**  
**ELECTE**  
**MAR 09 1994**  
**S F D**

*APPROVED FOR PUBLIC RELEASE; DISTRIBUTION UNLIMITED.*

**94-07617**



*copy*

**Rome Laboratory**  
**Air Force Materiel Command**  
**Griffiss Air Force Base, New York**

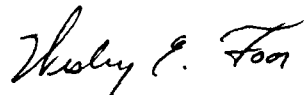
94 0 0 041

DTIC QUALITY ASSURED 6

This report has been reviewed by the Rome Laboratory Public Affairs Office (PA) and is releasable to the National Technical Information Service (NTIS). At NTIS it will be releasable to the general public, including foreign nations.

RL-TR-93-248 has been reviewed and is approved for publication.

APPROVED:



WESLEY E. FOER  
Project Engineer

FOR THE COMMANDER:



DONALD W. HANSON  
Director of Surveillance & Photonics

If your address has changed or if you wish to be removed from the Rome Laboratory mailing list, or if the addressee is no longer employed by your organization, please notify RL ( OCPA ) Griffiss AFB NY 13441. This will assist us in maintaining a current mailing list.

Do not return copies of this report unless contractual obligations or notices on a specific document require that it be returned.

# REPORT DOCUMENTATION PAGE

Form Approved  
OMB No. 0704-0188

Public reporting burden for this collection of information is estimated to average 1 hour per response, including the time for reviewing instructions, searching existing data sources, gathering and maintaining the data needed, and completing and reviewing the collection of information. Send comments regarding this burden estimate or any other aspect of this collection of information, including suggestions for reducing this burden, to Washington Headquarters Services, Directorate for Information Operations and Reports, 1215 Jefferson Davis Highway, Suite 1204, Arlington, VA 22202-4302, and to the Office of Management and Budget, Paperwork Reduction Project (0704-0188), Washington, DC 20503.

1. AGENCY USE ONLY (Leave Blank)		2. REPORT DATE December 1993		3. REPORT TYPE AND DATES COVERED Final Mar 93 - Nov 93	
4. TITLE AND SUBTITLE DEVELOPMENT OF PHASE-ONLY FILTERS FOR SENSOR IMAGERY				5. FUNDING NUMBERS C - F30602-93-C-0024 PE - 62702F PR - 4600 TA - P1 WU - PN	
6. AUTHOR(S) Samuel P. Kozaitis					
7. PERFORMING ORGANIZATION NAME(S) AND ADDRESS(ES) Florida Institute of Technology Division of Electrical & Computer Science & Engineering 150 W. University Blvd Melbourne FL 32901-6988				8. PERFORMING ORGANIZATION REPORT NUMBER N/A	
9. SPONSORING/MONITORING AGENCY NAME(S) AND ADDRESS(ES) Rome Laboratory (OCPA) 25 Electronic Pky Griffiss AFB NY 13441-4515				10. SPONSORING/MONITORING AGENCY REPORT NUMBER RL-TR-93-248	
11. SUPPLEMENTARY NOTES Rome Laboratory Project Engineer: Wesley E. Foor/OCPA/(315) 330-2944					
12a. DISTRIBUTION/AVAILABILITY STATEMENT Approved for public release; distribution unlimited.				12b. DISTRIBUTION CODE	
13. ABSTRACT (Maximum 200 words) We used the statistical technique of factor analysis to design binary and ternary optical correlation filters to identify objects in the presence of unknown or non-repeatable distortions. We considered values of spatial frequencies of training set imagery as features and used those spatial frequencies in our filter depending on their variation across a training set. In addition, we provided general expressions for performance measures as a function of training set imagery. The potential of our approach was evaluated with infrared sensor imagery that varied in an unknown way. Our statistically designed filters were easily calculated and performed well in the presence of noise. Furthermore, the performance of our filters were varied by allowing for trade-offs in performance measures. Our filters reduced the sensitivity of binary and ternary phase-only filters to changes in an object's appearance when the input imagery varied in an unknown manner.					
14. SUBJECT TERMS Optical filter design, Optical correlation, Optical pattern recognition				15. NUMBER OF PAGES 36	
				16. PRICE CODE	
17. SECURITY CLASSIFICATION OF REPORT UNCLASSIFIED	18. SECURITY CLASSIFICATION OF THIS PAGE UNCLASSIFIED	19. SECURITY CLASSIFICATION OF ABSTRACT UNCLASSIFIED	20. LIMITATION OF ABSTRACT UL		

## Abstract

We used the statistical technique of factor analysis to design binary and ternary optical correlation filters to identify objects in the presence of unknown or nonrepeatable distortions. We considered values of spatial frequencies of training set imagery as features and used those spatial frequencies in our filter depending on their variation across a training set. In addition, we provided general expressions for performance measures as a function of training set imagery. The potential of our approach was evaluated with infrared sensor imagery that varied in a unknown way. Our statistically designed filters were easily calculated and performed well in the presence of noise. Furthermore, the performance of our filters were varied by allowing for trade-offs in performance measures. Our filters reduced the sensitivity of binary and ternary phase-only filters to changes in an object's appearance when the input imagery varied in an unknown manner.

Accession For	
NTIS	CRA&I <input checked="checked" type="checkbox"/>
DTIC	TAB <input type="checkbox"/>
Unannounced <input type="checkbox"/>	
Justification	
By	
Distribution /	
Availability Codes	
Dist	Avail and/or Special
A-1	

## 1.0 Introduction

The primary difficulty with the use of binary phase-only filters (BPOFs) with sensor imagery in an optical correlator is the filter's sensitivity to changes in an object's appearance. In addition to these geometric distortions, the image of an object at a specific orientation can change due to effects such as lighting, weather and, especially in infrared imagery, the temperature differences between components of the object. The result is that object boundaries are often ambiguous or poorly defined in sensor imagery. If the global shape of an object is used for recognition, then changes in the imagery are often enough to significantly degrade the performance of a binary optical correlator.<sup>1</sup>

Because imagery from sensors often changes in an unknown way, a large number of reference images are needed to match an image in many applications when using a BPOF. Therefore, in an effort to make a binary optical correlator more practical, optical correlation filters that recognize objects varying in an unknown way is needed; filters should recognize objects in a training set as well as outside the training set.

Much work has been performed in designing distortion-invariant correlation filters,<sup>2-4</sup> but fewer methods exist for creating distortion-invariant BPOFs.<sup>5-7</sup> Generally, these approaches have been primarily used to identify or reject geometrically transformed versions of an object or to be robust in the presence of noise. Using these techniques, filters can be created that can perform well when the distortion can be well characterized.

Statistical approaches to distortion-invariant filter design have been previously used. For example, Kumar *et al.* modeled image differences of a training set as a stochastic process to design an optimal filter.<sup>8</sup> In another statistical approach, a linear transformation matrix was used to cluster all training vectors from each class to a single location in a reduced-dimensionality signal space.<sup>9</sup> The variance of time-sequenced correlation responses also has been examined to create a distortion-invariant filter.<sup>10</sup> However, by examining only the maxima of cross-correlation responses, little can be said about the behavior occurring at individual spatial frequencies.

Correlation filters can achieve improvements in signal-to-noise ratios (SNRs) by setting the filter to zero at particular spatial frequencies, which creates a ternary-valued filter.<sup>11,12</sup> In addition, this approach has had success in improving the distortion range and SNR of distortion-invariant BPOFs.<sup>13,14</sup> These methods set filter pixels to zero, based on

the ratio of the spectra of the noise to the composite filter image exceeding a specified threshold.

In contrast to previous attempts at distortion-invariant binary and ternary phase-only filter (POF) formulation, we developed a filter using a statistical technique whose values were determined by features of the training set. We attempted to find a filter that represented the critical characteristics of an object so that objects outside the training set could be identified. We examined an ensemble of BPOFs to select spatial frequencies that would recognize images outside of our ensemble. Because correlation filters are derived from the Fourier transform of an object, we examined feature extraction in the Fourier domain. We considered the BPOFs of input images as a set of features to recognize objects and used a statistical approach to examine features that were invariant with respect to the training set. Similar approaches have been used to perform feature extraction with optical processors.<sup>15,16</sup> We retained those Fourier features that were invariant among a training set and set to zero those that varied using a technique similar to factor analysis to design a ternary filter.<sup>17</sup>

In the next section we describe our approach for the statistical design of distortion-invariant binary and ternary POFs based on features of a training set. Section 3 contains computer simulations using our statistically designed filter, along with results from our attempt to increase the SNR. Finally, our conclusions follow in section 4.

## **2.0 Statistical binary and ternary phase-only filters**

### **2.1 Filter development**

We used features of training images to design both binary and ternary POFs. To construct our filter, we considered a signal space where each feature of an image was represented as an axis. The position along an axis represented the value of that feature. For a set of training images in the same class, we examined the variance of the values of each feature. We eliminated features associated with large variances by setting the value of that feature to zero. In this way, we formed a cluster of training images in a reduced dimensionality feature space. We then chose a set of features that best represented our cluster.

Because BPOFs of objects have been sufficiently descriptive in many binary optical pattern recognition experiments, we considered the BPOF of a training image as a collec-

tion of characteristic features. Therefore, each axis in our signal space was represented by a discrete spatial frequency. The position along an axis represented the coefficient of the discrete Fourier transform (DFT) at that spatial frequency.

There are different ways to create a BPOF of an object.<sup>18,19</sup> We used a common method to create BPOFs where the phase was set to  $\pm 1$  at each pixel according to

$$H_i[n, m] = \begin{cases} 1 & \text{if } 0 \leq \phi_i[n, m] < \pi \\ -1 & \text{if } \pi \leq \phi_i[n, m] < 2\pi \end{cases}, \quad (1)$$

where  $H_i[n, m]$  was the BPOF of the  $i$ th training image,  $\phi_i[n, m]$  was the phase of the complex conjugate of  $S_i[n, m]$ , and  $S_i[n, m]$  was the DFT of the  $i$ th training image. If the calculated phase angle was between 0 and  $\pi$ , the phase at that pixel was set to +1. If the calculated phase angle was between  $\pi$  and  $2\pi$ , the phase at that pixel was set to -1.

The Fourier coefficients of the training images were examined over the training set on a pixel-by-pixel basis in terms of their similarity, with the distance in signal space between Fourier coefficients as a measure of their similarity. The smaller the distance the more similar the coefficients. Because we used BPOFs, only two possible values existed for an individual pixel. If values of two BPOFs corresponding to the same pixel were the same, we described the distance between them as -1; if the values were different, we considered the distance as +1. The distances between coefficients of two BPOFs were described as

$$d_{i,j}[n, m] = H_i[n, m] \oplus H_j[n, m], \quad (2)$$

where  $H_i[n, m]$  and  $H_j[n, m]$  represented two BPOFs of the training set,  $n$  and  $m$  were discrete spatial frequencies, and  $\oplus$  was the exclusive-OR (XOR) function. The coefficient at each pixel of the BPOFs are  $\pm 1$ ; therefore, we used  $\pm 1$  in Eq. (2) to represent Boolean values. In this way, the similarity of two BPOFs were determined, and  $d_{i,j}[n, m]$  was represented as an array of  $\pm 1$ s.

We measured the similarity of BPOFs across the entire training set. We measured the distances between coefficients of BPOFs of each training image and every other training image. We summed all the distances on a pixel-by-pixel basis and used this quantity as a measure of the clustering of values for a particular spatial frequency. We used the criterion function<sup>20</sup>

$$J[n, m] = \frac{1}{N^2} \sum_{i=1}^N \sum_{j=1}^N d_{i,j}[n, m] \quad (3)$$

to measure the clustering of distances, where  $N$  was the number of images in the training set. A more compact cluster was indicated by a more negative value at a particular  $n$  and  $m$ .

By removing redundant calculations from Eq. (3), the clustering was ultimately represented in a simpler way. For example, the distance between a filter and itself yielded an array of -1s. In addition, the XOR function is commutative, and the distances between two filters had to be calculated only once. We found that the clustering of distances of the training set could be represented simply by a summation of BPOF coefficients across the training set. The clustering was represented by the function  $\bar{J}[n, m]$  as

$$\bar{J}[n, m] = \sum_{i=1}^N H_i[n, m], \quad (4)$$

where  $\bar{J}[n, m]$  indicated that a more compact cluster was indicated by larger values. This was in contrast to  $J[n, m]$ , where a more compact cluster was indicated by smaller values.

Our main objective was to recognize images in the training set as well as images outside the training set that are of the same class. Therefore, we selected a filter that retained features (spatial frequencies) that were most consistent across a training set. Because we have a measure of the clustering of features in Eq. (4), we retained only those features that



were most compactly clustered in signal space. Using this approach, we expected objects with the same features as our training set to be recognized by our filter.

We used factor analysis<sup>21</sup> to retain spatial frequencies of our training set that were more compactly clustered than others. The goal of factor analysis is to account for a process by a reduced number of variables. The basis of factor analysis requires an assumption that a process can be broken down into additive parts.<sup>21</sup> Because the process, the cross-correlation of a training image and a composite filter  $H[n,m]$ , can be written in a discretized form as the summation

$$c_{0i} = \sum_{n,m} S_i[n,m] H[n,m], \quad (5)$$

where  $c_{0i}$  was the correlation peak value for the  $i$ th centered training image, the basic assumption of factor analysis was satisfied. The spatial frequencies were variables,  $H[n,m]$  was the factor at  $n$  and  $m$ , and  $S_i[n,m]$  was the factor at  $n$  and  $m$ , in the  $i$ th variate. In factor analysis, usually  $H[n,m]$  would be known,  $S_i[n,m]$  would be estimated, and the  $S_i[n,m]$ 's that account for the most significant variation of  $c_{0i}$  would be retained.

In contrast to factor analysis, we sought to retain variables  $n$  and  $m$  that did not significantly vary  $c_{0i}$ . Therefore, we eliminated the spatial frequencies whose coefficients had large distances over a training set. For example, small values of  $\bar{J}[n,m]$  showed that some BPOF coefficients were not consistent over a training set. We described our resulting filter as

$$G_\alpha[n,m] = \begin{cases} 1 & \text{if } \bar{J}[n,m] \geq p \\ -1 & \text{if } \bar{J}[n,m] \leq -p \\ 0 & \text{otherwise} \end{cases}, \quad (6)$$

where  $p$  was a threshold, and  $\alpha = p/N$  was a factor that indicated the minimum percentage of features across the training set that had the same value.

The number of possible different filters depended on the number of images in the training set. The variable  $p$  could take values from  $0 \leq p \leq N$ . To describe different filters with each value of  $p$  and to avoid choosing a value for  $G_{\alpha}[n,m]$  when  $\bar{J}[n,m]$  was 0,  $p$  should be odd if  $N$  is odd, and  $p$  should be even if  $N$  is even. The number of different possible filters for a given  $N$  was described as

$$N_{filter} = \begin{cases} \frac{N}{2} & N \text{ even} \\ \frac{N}{2} + \frac{1}{2} & N \text{ odd} \end{cases} \quad (7)$$

## 2.2 Performance measures

We primarily considered the SNR and the peak-to-correlation energy (PCE) as measures of performance.<sup>22</sup> The SNR is defined as

$$SNR = \frac{|E\{c_0\}|^2}{var\{c_0\}} \quad (8)$$

where  $c_0$  is the correlation peak value for a centered in-class image,  $E\{\}$  is the expected value and  $var\{\}$  is the variance. The SNR is often calculated using independent noise samples over several measurements because noise will make the correlation result change between samples. In our approach, we had two independent sources contributing to the change in the correlation result: differences between training images for unknown reasons, and additive noise due to the sensor or correlator system. As a result, the SNR will be finite without additive noise present. Consistent with Eq. (5), we considered  $S[n,m]|_{n,m}$  to be a random variable with an expected value and variance. Therefore, the maximum value of Eq. (8) without additive noise present was written in a discretized form as

$$SNR =$$

$$\frac{\left| \sum_{n,m} E\{S[n,m]\} G_{\alpha}[n,m] \right|^2}{\sum_{n,m} [G_{\alpha}[n,m]]^2 \text{var}\{S[n,m]\} + 2 \sum_{n,m} \sum_{n',m'} G_{\alpha}[n,m] G_{\alpha}[n',m'] \text{cov}\{S[n,m], S[n',m']\}} \quad (9)$$

where  $\text{cov}\{\}$  was the covariance and  $n, m < n', m'$ . When samples of  $S[n,m]$  are uncorrelated, Eq. (9) reduces to

$$SNR = \frac{\left| \sum_{n,m} E\{S[n,m]\} G_{\alpha}[n,m] \right|^2}{\sum_{n,m} [G_{\alpha}[n,m]]^2 \text{var}\{S[n,m]\}} \quad (10)$$

In the presence of additive noise,  $S[n,m]$  may be replaced by  $S[n,m] + P[n,m]$ , where  $P[n,m]$  is the power spectral density of the noise. Eq. (10) becomes

$$SNR = \frac{\left| \sum_{n,m} E\{S[n,m]\} G_{\alpha}[n,m] \right|^2}{\sum_{n,m} [G_{\alpha}[n,m]]^2 \text{var}\{S[n,m]\} + \sum_{n,m} P[n,m] [G_{\alpha}[n,m]]^2} \quad (11)$$

The PCE can be used as a measure of sharpness of the correlation peak and was expressed as

$$PCE = \beta \frac{|\sum S_i[n, m] G_\alpha[n, m]|^2}{\sum |S_i[n, m]|^2 |G_\alpha[n, m]|^2} \quad (12)$$

for a particular  $S_i[n, m]$ .

### 3.0 Computer simulations

Infrared (IR) imagery (8-14  $\mu\text{m}$ ) of ground scenes from actual sensors were used to generate and evaluate filters. Images were digitized with 128 x 128 pixels with 8 bits/pixel. Thresholding was performed by choosing a single threshold value for the entire image. In the imagery we examined, the background and object were easily separated; however, edges were not well-defined. As variables such as lighting, noise, and atmospheric effects within an image changed, the resulting thresholded images would have remained similar but different. We used objects of the same scale and rotation to examine the effects of unknown variations of the inputs.

We used 15 uncorrelated training images that came from thresholded sensor imagery to generate different statistical filters, one for each possible value of  $\alpha$ . Five of the 15 images are shown in Fig. 1. A total of eight filters were produced with values of  $\alpha = 0.07, 0.20, 0.33, 0.47, 0.6, 0.73, 0.87, \text{ and } 1.00$ . The support functions of the filters, the region where the filter was transmitting, are shown in Fig. 2, where white regions indicate the transmitting areas. The support function when  $\alpha = 0.07$  is not shown because all pixels were transmitting. We evaluated our statistical filters using images from the training set and additional imagery. We used both types of imagery, objects that were not in the training set but in the same class and noisy versions of the same images.

#### 3.1 Test imagery performance

Using the training set, we found the SNR, PCE, normalized correlation heights, and transmitting pixels for statistically-designed filters of different  $\alpha$ , which are summarized in Table 1. The correlation heights were normalized by setting the maximum correlation height for each filter equal 100. Furthermore, the value of  $\beta$  in Eq. (12) was set to an arbitrary constant. In general, the SNR increased as  $\alpha$  increased, while the maximum SNR of

258 occurred at  $\alpha = 0.73$ . In addition, as  $\alpha$  increased, the PCE decreased. The results showed that the correlation responses became broader but more consistent as  $\alpha$  increased.

We compared the results of our statistically-designed filters to that of an fSDF filter. An fSDF filter is an iteratively designed, equal-correlation peak filter that takes into account spatial light modulator (SLM) modulation characteristics.<sup>5</sup> Therefore, an fSDF filter was designed to produce equal correlation heights for the training set using a BPOF. The average PCE value of the training set using the fSDF filter was 140.7, which was higher than the values obtained with the statistically designed filters.

For correlation filters to be the most useful with sensor imagery, they should recognize objects in the same class as, but not in, the training set. Therefore, we used the same type of imagery from which the training set was gathered, but we used a different photograph to generate 10 additional test objects in the same class as the training set. Furthermore, we used an additional nine objects that visually appeared similar to the training set but were in a different class to help evaluate the discrimination of our filters. We labeled those images that were not in the same class as the training set as images 26 - 29. Four of these images are shown in Fig 3. A summary of the cross-correlation results for this additional imagery using the filters in the previous experiment are shown in Table 2. The data showed that the SNRs resulting from differences in the correlation heights of the 25 in-class images generally increased as  $\alpha$  increased and were higher than the fSDF filter's response for most values of  $\alpha$ . The average normalized correlation heights, using in-class imagery not in the training set demonstrated similar behavior. In addition, the PCE of the statistical filters were sometimes comparable but always lower than the fSDF filter. We used the ratio of the averages of the normalized correlation heights of the in-class to out-of-class images as a measure of discrimination. This ratio was always higher with the fSDF filter but comparable to the statistical filters in most cases.

### 3.2 Noise performance

We repeated the previous experiments using the same filters but with noise added to all test images. Ten percent of the pixels in each test image were randomly selected and changed in value to represent noise. The previous experiments were performed with noisy images, and the results were summarized in Table 3. We compared the performance of the statistical filters to a ternary version of an fSDF filter specifically designed for improved SNR values in the presence of noise (referred to as a TSDF<sub>SNR</sub> filter).<sup>14</sup> For the statistical

filters, the SNRs and normalized correlation heights generally increased as  $\alpha$  increased. The SNRs of the statistical filters were higher than the TSDF<sub>SNR</sub> filter for most values of  $\alpha$ . The normalized correlation heights of the training and in-class images for the statistical filters were always higher than for the TSDF<sub>SNR</sub> filters. In addition, the ratios of the in-class to out-of-class correlation heights were more similar for the two different types of filters than the noise-free case.

### 3.3 Improved SNR

We used an algorithm that has been successfully used to design optimal POFs for additive noise<sup>12</sup> to increase the SNR of our statistical filters. We sorted the values of  $|E\{S[n,m]\}|$  after forming the product with a  $G_\alpha[n,m]$ ; different thresholds were used to determine support functions for a particular  $\alpha$ . All possible support functions were found from each  $G_\alpha[n,m]$  and described as

$$R_\alpha = \{n, m; |E\{S[n, m]\}| |G_\alpha[n, m]| > T\} \quad (13)$$

where  $T$  was a threshold. We found the maximum SNR and corresponding support function. The SNR and PCE as a function of transmitting pixels according to Eq. (13) for filters of different  $\alpha$  are shown in Fig. 4. In all cases, the results show that the highest SNR values occurred at relatively low PCE values.

In some applications the low PCE may be unacceptable. Because SNR values were often satisfactory for a variety of transmitting pixels, a filter may be chosen that is not optimal in terms of SNR and PCE but may yield a satisfactory compromise.

To view the filters in terms of both SNR and PCE performance, we created a scatter diagram in Fig. 5 that showed the SNR as a function of PCE. From this diagram, the filter that had the highest SNR for a given value of PCE can be chosen. Filters calculated from Eq. (6) without any SNR improvement are indicated by circles around their data points in Fig. 5. Note that these filters occurred at the maximum PCE for a given  $\alpha$ . Furthermore, some filters with different  $\alpha$ 's appeared to offer similar performance.

## 4.0 Experiment

We used an optical correlator that is described in more detail in the appendix.

The experimental results for the statistical filter for  $\alpha = 0.07$  both when noise was, and was not present are shown in Table 4. The main difference between the experimental and simulated data was that the values of the correlation heights were more consistent in the experimental data. It appeared that this was due to noise associated with the SLM. When an image was written to an SLM, a small percentage of the pixels (about 5%) didn't display the values intended. This is important because of the sensitivity of the BPOF to changes in an input. The results showed that the correlation heights of the training set were less than expected but were more consistent.

## 5.0 Conclusions

The feature that contributed most to the improvement in SNR of correlation filters when compared to other designs was the statistical design methodology. This method differs from others by using a statistical approach to identify spatial frequencies useful to increase the probability of recognition of in-class objects, especially those not in the training set. The performance of the statistically-designed BPOFs depended on a parameter  $\alpha$ . The SNR and normalized correlation heights of objects generally increased as  $\alpha$  increased. In most cases, the SNR and normalized correlation heights of the statistically-designed filters was higher than both the fSDF and TSDF<sub>SNR</sub> filters. Similar results were found when the statistical filters were tested with noisy test images.

Another feature of our approach that contributed to the improvement of SNR filters was the retention of spatial frequencies based on their magnitude. By combining this method with our statistical approach, we could maximize the SNR for a given value of PCE.

The statistically designed filters were more easily calculated than both fSDF and TSDF<sub>SNR</sub> filters. The statistical filters required calculating  $N$  FFTs. In contrast, the fSDF approach required a cross-correlation between every training image and filter for every iteration. This approach requires  $NI$  FFT calculations, where  $I$  is the number of iterations and generally has been set to  $10$ .<sup>2</sup> The TSDF<sub>SNR</sub> filter required  $2NI$  FFT calculations.

Therefore, the time and number of operations required to calculate our statistical filters were about an order of magnitude less than that of the fSDF and TSDF<sub>SNR</sub> filters.

The sensitivity of a BPOF to changes in an object's appearance is a significant factor when attempting to recognize nondeterministic objects of the same class. Eliminating properly selected spatial frequencies can reduce this sensitivity. However, this will affect discrimination. In our experiments, the ratios of correlation heights for in-class to out-of-class images were generally lower for the statistically-designed filters when compared to other approaches. In addition, correlation responses were generally less sharp and the light efficiency was lower for the statistical filters when compared to other approaches.

Correlation is a basic operation that is required by nearly all machine vision and pattern recognition systems. As larger and faster input sensors are used, the speed of electronic systems is stretched to beyond its limit. By utilizing the massive parallelism and high bandwidth offered by the optics technology, much more data can be processed at higher rates. The optical correlator presents a nearly mature technology that needs work in the areas of device development and system packaging for uses in either military or civilian applications. A growing number of manufacturing industries are looking towards machine vision to improve the performance and capabilities of automated assembly lines and inspection techniques.

It is recommended that for objects to be recognized from sensor imagery using an optical correlator, emphasis should be placed on reducing the trade-offs between robustness, and discrimination, and light efficiency.



## Appendix

This appendix describe some important characteristics of the correlator such as the experimental apparatus, the alignment, and the controlling and displaying of images. The correlator uses binary SLMs, so we used binary phase-only filters. Images and filters were generated on a computer and put in the proper format for display on the SLMs. The system is a research platform so it may need realignment from time to time, or some procedures may seem cumbersome.

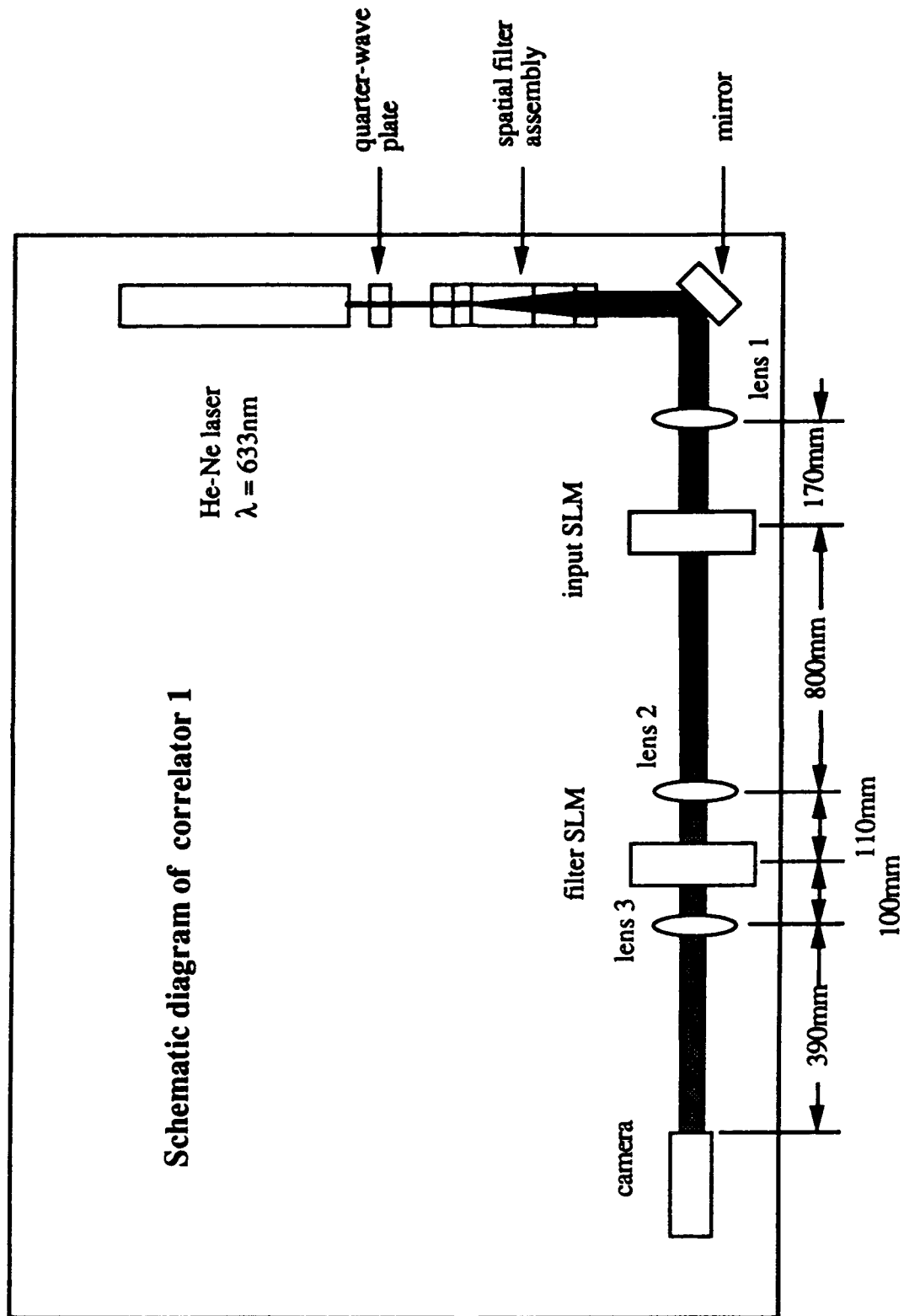
We used two set -ups that were pretty much the same in terms of performance. We first set -up a correlator using a He-Ne laser because of the known good beam quality of this device. Because the SLMs used were highly attenuating, the correlation result was often dim. More powerful He-Ne lasers ( $>15\text{mW}$ ) are typically quite long, so we used a compact higher power frequency-doubled YAG ( $\lambda=532\text{nm}$ ) laser in another set-up.

The laser in the first set-up was a Mellis Griot linearly polarized He-Ne operating at a wavelength of  $633\text{nm}$ ; we measured  $13\text{mW}$  at the output of the laser. The spatial filter assembly was made by Newport and consisted of: a  $40\times$  microscope objective,  $10\text{mm}$  pinhole, and  $250\text{mm}$  focal length collimating lens. The correlation result can often be quite dim, especially when using the framegrabber to capture a result; therefore, sometimes a  $20\times$  objective was used or we removed the pinhole. The mirror is oriented at about  $45$  degrees and is used simply to bend the beam around the optical bench. Unfortunately, the mirror may produce an elliptically polarized reflected beam from the linearly polarized incident beam.

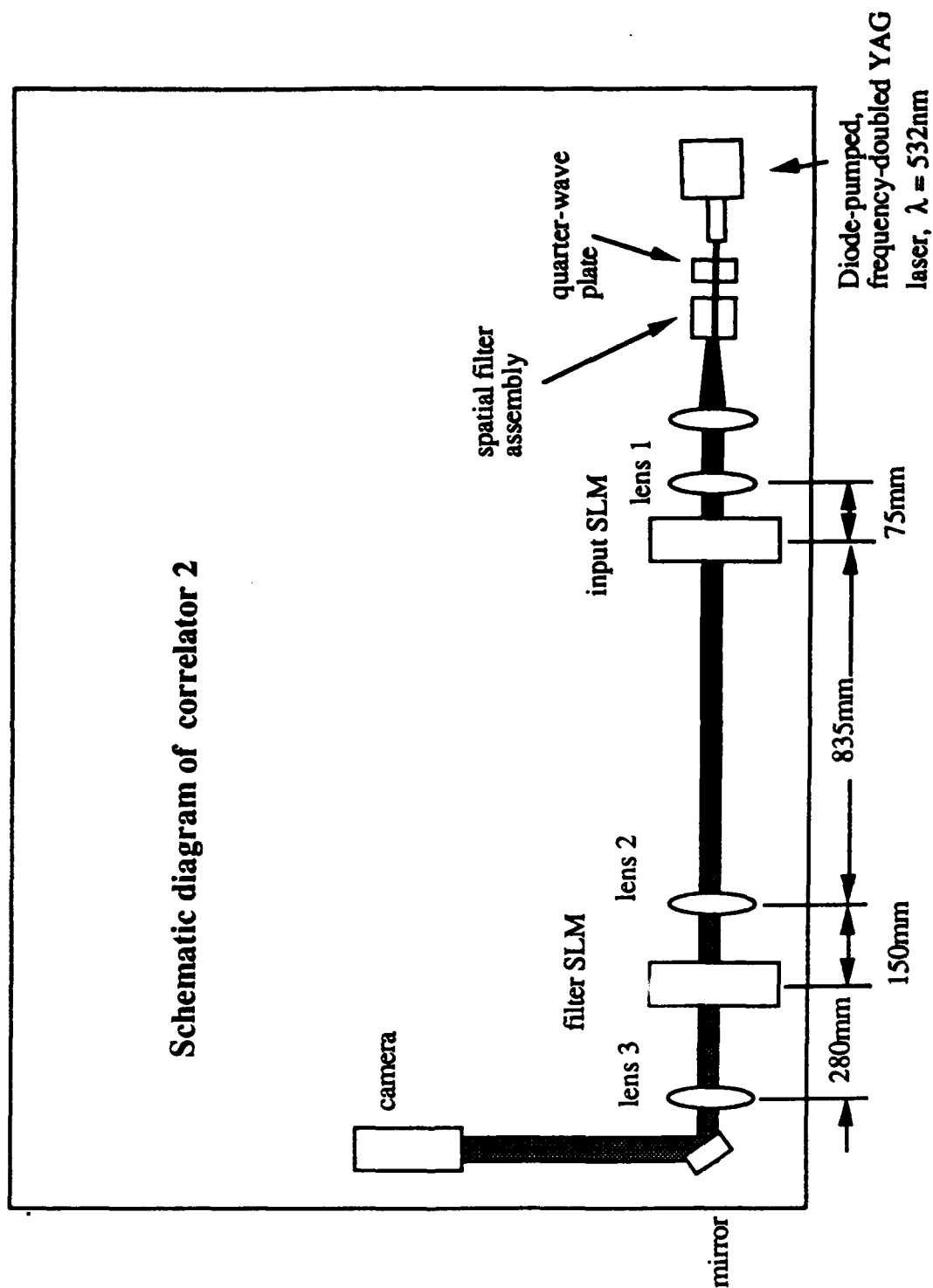
The laser in the second set-up was a Adlas 200 diode-pumped, frequency doubled YAG laser operating at a wavelength of  $532\text{nm}$ . The spatial filter assembly was made by Newport and consisted of: a  $20\times$  microscope objective,  $10\text{mm}$  pinhole, and  $250\text{mm}$  focal length collimating lens. We found that the pinhole must be used for meaningful results.

The elliptically polarized beam can be compensated for with a quarter-wave plate (the light entering the SLM should be linearly polarized). To determine if a quarter-wave plate is needed, a polarizer should be placed temporarily in the beam after being reflected from the mirror. The polarizer should be rotated so that the beam intensity is a minimum. If this minimum is different than the minimum obtained with the polarizer placed before the mirror, then the beam may need to be compensated.

Schematic diagram of correlator 1



**Schematic diagram of correlator 2**



To adjust the quarter-wave plate, place the polarizer after the mirror and adjust it so that it produces a minimum. Then place the quarter-wave plate in the path of the beam before the mirror. Rotate the quarter-wave plate so that a minimum is obtained at the out-

put of the polarizer. Now the light entering the input SLM is linearly polarized. The quarter-wave plate produces an elliptically polarized beam that is cancelled by the mirror. We found that for the second set-up, the quarter-wave plate was mandatory.

The input SLM is imaged onto the filter SLM by lenses 1 and 2. The calculation of the effective focal length required and the alignment procedure will be discussed in the following paragraphs. The effective focal length required was 1168mm for set-up 1 and 1340mm for set-up 2. It's difficult to find a lenses of exactly these focal lengths, so we used two lenses. In addition, the SLM should be placed a distance equal to a focal length before the Fourier transform lens for best imaging. Our experience shows that this requirement can be relaxed; besides, such a system takes up more space and needs more mirrors. We both set-ups we used an achromatic lens of  $f = 1000\text{mm}$  for lens 1 and a plano-concave lens of  $f = -250\text{mm}$  for lens 2.

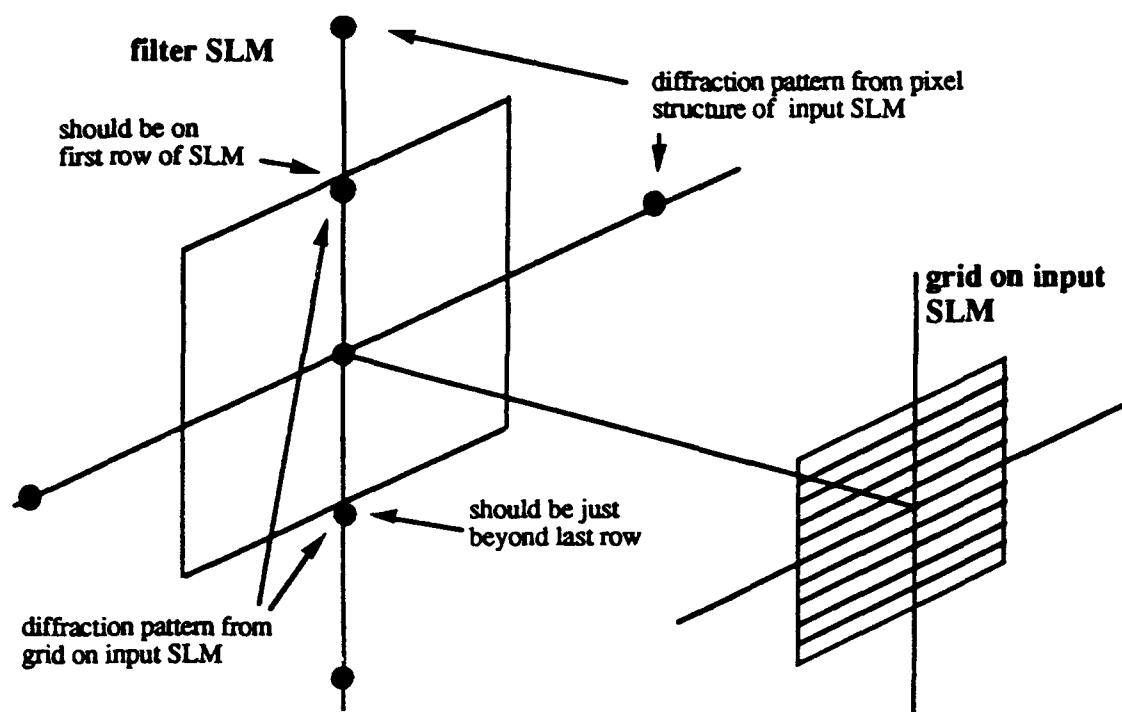
The input SLM is operated in a maximum contrast mode. That means that the background of an image displayed on the SLM is adjusted (with the polarizer on the SLM) so that a minimum of light comes through.

The filter SLM is operated in a phase-only mode. To adjust the filter SLM to operate in the phase-only mode, the light from the input SLM must be incident on the filter SLM. When rotating the polarizer on the filter SLM, there is a region where the pattern on the filter SLM quickly "flips"; regions on the SLM that were transmitting become opaque and vice versa. The point in between these different contrast modes where there is no contrast is the phase-only point of operation.

The correlator is a relatively simple device; however, its alignment is critical. The most critical factor in its alignment is the imaging of the input SLM onto the filter SLM. The rule that governs this part of the alignment is that the highest spatial frequency of the input SLM should be imaged onto the edge of the filter SLM. Therefore, the focal length of the Fourier Transform lens should be<sup>23</sup>

$$f = Nd_2d_1/\lambda \quad (14)$$

where  $N$  is the number of pixels along a side of the filter SLM (128),  $d_2$  and  $d_1$  are the center-to-center spacing of the pixels of the filter and input SLMs respectively (76mm), and  $\lambda$  is the wavelength of light being used. The highest spatial frequency grid should be placed on the input SLM. The grid will be rows of dark, light, dark, light, etc. The input SLM and the lenses should be adjusted so that the first diffraction order due to the pattern on the input SLM is on the edge of the filter SLM.



The two Semetex SLMs the correlator uses are made by the same company but share little between them. The devices use different software, are driven by different cards, and accept different types of file formats for images that may be displayed on them. The SLM in the filter plane is an "older" device of 128 x 128 pixels and the SLM in the input plane is a "newer" device 256 x 256 pixels. The newer devices do not display an intricate pattern as reliably as the old devices do. This is important for a filter SLM because the pattern is usually intricate. Therefore, we use the old device in the filter plane. In addition, the image displayed on the input SLM should only occupy 128 x 128 pixels or distortion and an overlapping of the correlation responses will result. Finally, it's not clear what must be

done to drive both devices from the same computer. There may be a conflict with the driver boards but this problem should not prove too difficult. However, we currently use a separate computer to drive each SLM.

There exists some compatibility problems with generating an image to be displayed on an SLM and then actually having it displayed. This problem arises because the SLMs must be driven with IBM-compatible computers, and image manipulation and generation has often been performed on the Macintosh. The IBM computers have generally been harder to work with than the Macintosh in terms of the graphics needed to generate images and filters. Maybe in the future, all development of imagery and filters could be done on the IBM machines, but that is not the case now.

Although some compatibility problems exist, they are not prohibitive. Software has been developed to help ease the transfer of Macintosh images to the proper format for the IBM. Let's start with the IBM computers and examine how we can display images on the SLMs. We'll discuss the specific programs to drive the SLMs later, an important factor is that an image to be displayed on an SLM must be in the proper format, the .bnd format for the old device (filter plane) or the .scn format for the new device (input plane). Because the Macintosh has been so useful in generating images, more effort has been put into converting Macintosh images.

## 6.0 References

- [1] S. P. Kozaitis, and W. E. Foor, "Performance of synthetic discriminant functions for binary phase-only filtering of thresholded imagery," *Optical Engineering* 31(4), 830-837 (1992)
- [2] C. F. Hester, and D. Casasent, "Multivariant technique for multiclass pattern recognition," *Applied Optics* 19, 1758-1761 (1980)
- [3] Z. Bahri, and B. V. K. Vijaya Kumar, "Generalized synthetic discriminant functions," *J. Opt. Soc. Amer. A* 5(4), 562-571 (1988)
- [4] B. V. K. Vijaya Kumar, "Tutorial survey of composite filter designs for optical correlators," *Applied Optics* 31(23), 4773-4801 (1992)
- [5] D. A. Jared, and D. J. Ennis, "Inclusion of filter modulation in synthetic discriminant function construction," *Applied Optics* 28(2), 232-239 (1989)
- [6] Z. Bahri, and B. V. K. Vijaya Kumar, "Algorithms for designing phase-only synthetic discriminant functions," in *Optical Information Processing Systems and Architectures*, B. Javidi, ed., Proc. SPIE 1151, 138-147 (1989)
- [7] R. R. Kallman, "The construction of low noise correlation filters," *Applied Optics* 25, 1032-1033 (1986)
- [8] B. V. K. Vijaya Kumar, D. Casasent, and A. Murakami, "Principle-component imagery for statistical pattern recognition correlators," *Optical Engineering* 21(1), 43-47 (1982)
- [9] Z. H. Gu, J. H. Leger, and S. H. Lee, "Optical implementation of the least-squares linear mapping technique for image classification," *J. Opt. Soc. Amer.* 72, 787-7931 (1982)
- [10] T. R. Walsh, and M. K. Giles, "Statistical filtering of time-sequenced correlation responses for distortion-invariant recognition of multiple input objects," *Optical Engineering* 29(9), 1052-1064 (1990)
- [11] D. L. Flannery, J. S. Loomis, and M. E. Milkovich, "Transform-ratio ternary phase-amplitude formulation for improved correlation discrimination," *Applied Optics* 27(19), 4079-4083 (1988)

- [12] B. V. K. Vijaya Kumar, and R. D. Juday, "Design of phase-only, binary phase-only, and complex ternary matched filters with increased signal-to-noise ratios for colored noise," *Optics Lett.* 16(13), 1025-1027 (1991)
- [13] M. E. Milkovich, D. L. Flannery, and J. S. Loomis, "Transform-ratio ternary phase-amplitude filter formulations for character recognition," *Optical Engineering* 28(5), 487-493 (1989)
- [14] J. D. Downie, "Case study of binary and ternary synthetic discriminant function filters with similar in-class and out-of-class images," *Optical Engineering* 32(3), 560-570 (1993)
- [15] D. Clark, and D. P. Casasent, "Practical optical Fourier analysis for high speed inspection," *Optical Engineering* 27(5), 365-371 (1988)
- [16] D. P. Casasent, and V. Sharma, "Feature extractors for distortion-invariant robot vision," *Optical Engineering* 23(5), 492-498 (1984)
- [17] S. P. Kozaitis, R. H. Cofer, and W. E. Foor, "Statistical design of ternary phase-only filters for distortion invariance," *Optics Communications* (accepted for publication 1993)
- [18] M. W. Farn, and J. W. Goodman, "Optimal binary phase-only matched filters," *Applied Optics* 27(21), 4431-4437 (1988)
- [19] R. R. Kallman, "Optimal low-noise phase-only and binary phase-only optical correlation filters for threshold detectors," *Applied Optics* 25(23), 4216-4217 (1986)
- [20] R. O. Duda, and P. E. Hart, *Pattern Classification and Scene Analysis*, Wiley:New York (1973)
- [21] D. N. Lawley, and M. A. Maxwell, *Factor Analysis as a Statistical Method*, Butterworths: London (1963)
- [22] B. V. K. Vijaya Kumar, and L. Hasselbrook, "Performance measures for correlation filters," *Applied Optics* 29(20), 2997-3006 (1990)
- [23] J. A. Davis, M. A. Waring, G. W. Bach, R. A. Lilly, and D. M. Cottrell, "Compact optical correlator design," *Applied Optics* 28(1) 10-11 (1989)



**TABLE 1. Performance of statistically designed filters for images in training set**

	Statistical filter							
	$\alpha=0.07$	$\alpha=0.2$	$\alpha=0.33$	$\alpha=0.47$	$\alpha=0.6$	$\alpha=0.73$	$\alpha=0.87$	$\alpha=1.00$
Transmitting pixels	16384	11276	7037	4220	2931	1858	1324	918
SNR of training set	65.6	79.8	99.2	144	214	258	222	202
Avg. PCE of training set	131	136	131	113	94.6	92.5	82.3	67.4
Avg. normalized correlation height of training set	75.1	75.7	81.4	82.9	84.0	84.8	87.2	88.9

**TABLE 2. Performance of filters for images of in-class and out-of class sets**

	Statistical filter								fSDF filter
	$\alpha=0.07$	$\alpha=0.2$	$\alpha=0.33$	$\alpha=0.47$	$\alpha=0.6$	$\alpha=0.73$	$\alpha=0.87$	$\alpha=1.00$	
SNR of in-class set	27.0	30.1	40.9	52.8	86.1	86.7	86.5	80.6	45.7
Avg. PCE of in-class set	86.8	90.7	88.2	76.8	64.8	62.9	56.7	46.4	90.8
Avg. normalized correlation height of in-class images (not in training set)	48.0	49.5	59.4	65.6	72.2	76.5	76.6	75.7	58.8
Ratio of average in-class to out-of-class correlation heights	3.88	3.97	4.67	4.82	4.49	4.11	3.76	3.39	6.00

**TABLE 3. Normalized correlation heights for filters using images with 10% noise**

	Statistical filter								TSDF <sub>SNR</sub> filter
	$\alpha=0.07$	$\alpha=0.2$	$\alpha=0.33$	$\alpha=0.47$	$\alpha=0.6$	$\alpha=0.73$	$\alpha=0.87$	$\alpha=1.00$	
SNR of training set	53.4	68.5	80.4	110	195	209	185	200	70.1
Avg. normalized correlation height of training set	62.2	53.0	52.6	55.2	59.2	61.0	60.4	62.9	33.9
SNR of in-class set	21.9	27.0	37.8	48.6	52.9	71.5	77.0	72.7	63.9
Avg. normalized correlation height of in-class images (not in training set)	40.0	38.7	47.4	47.2	47.4	53.3	53.8	53.9	30.9
Ratio of average in-class to out-of-class correlation heights	2.20	2.65	3.69	2.97	3.11	3.22	3.44	3.21	3.68

**TABLE 4. Experimental results for  $\alpha = 0.07$**

	Statistical filter	
		10% noise
SNR of training set	102	65.7
Avg. normalized correlation height of training set	90.8	73.4
SNR of in-class set	32.7	30.5
Avg. normalized correlation height of training set (not in training set)	1.77	1.43



**Image 1**



**Image 2**



**Image 3**

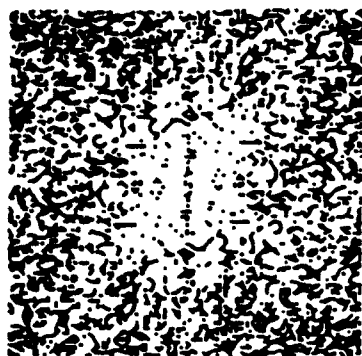


**Image 4**

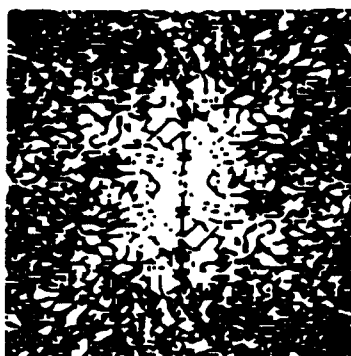


**Image 5**

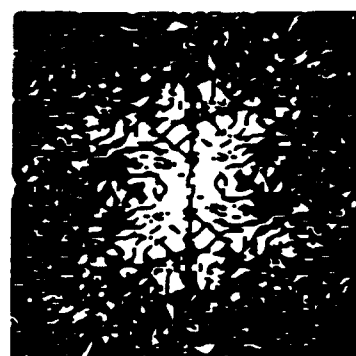
**FIGURE 1. Examples of images used in training set obtained from sensor data.**



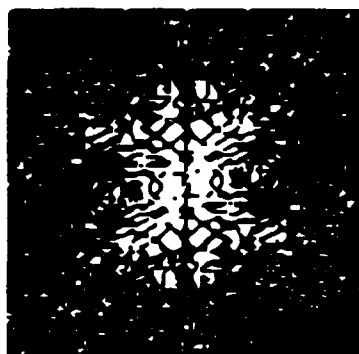
$\alpha = 0.2$



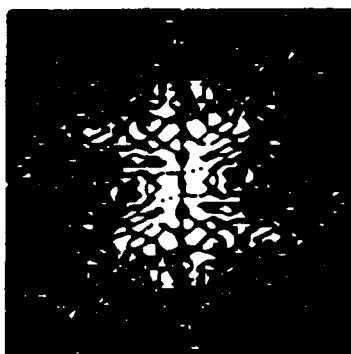
$\alpha = 0.33$



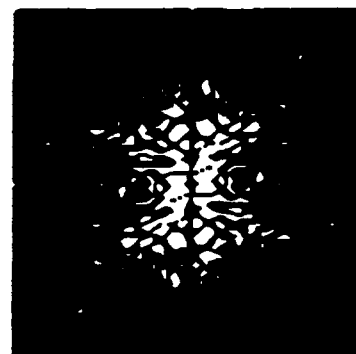
$\alpha = 0.47$



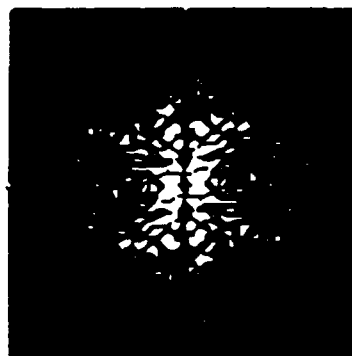
$\alpha = 0.6$



$\alpha = 0.73$



$\alpha = 0.87$



$\alpha = 1.0$

FIGURE 2. Support functions for training set from Eq. (6).



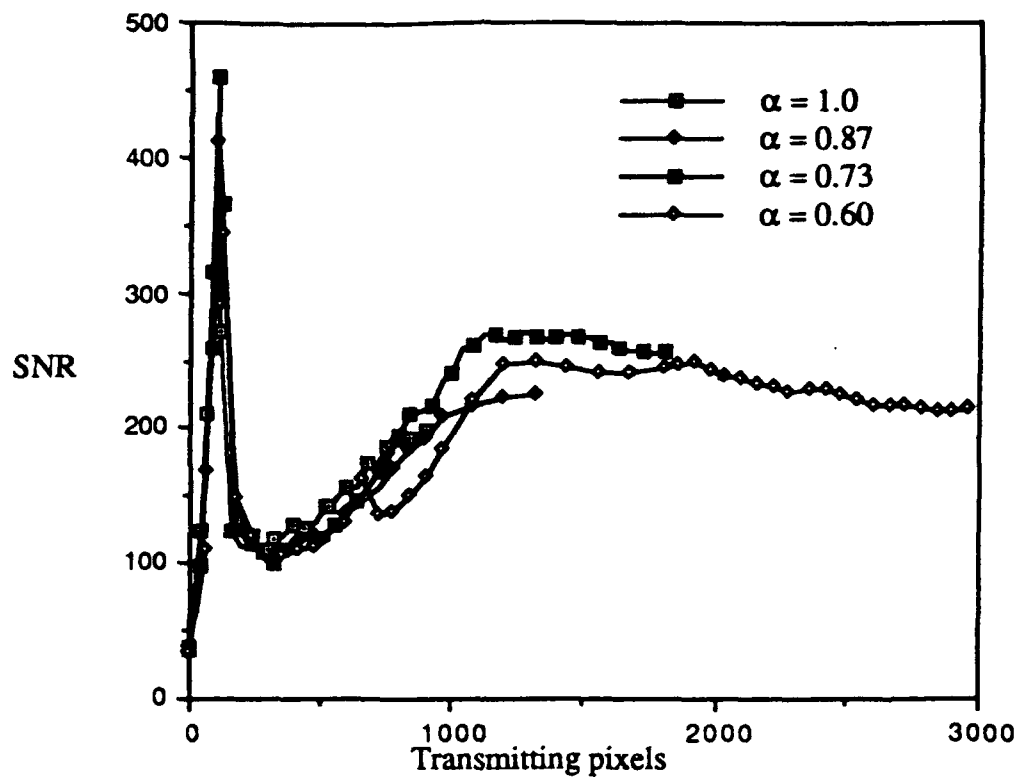
Image 26

Image 27

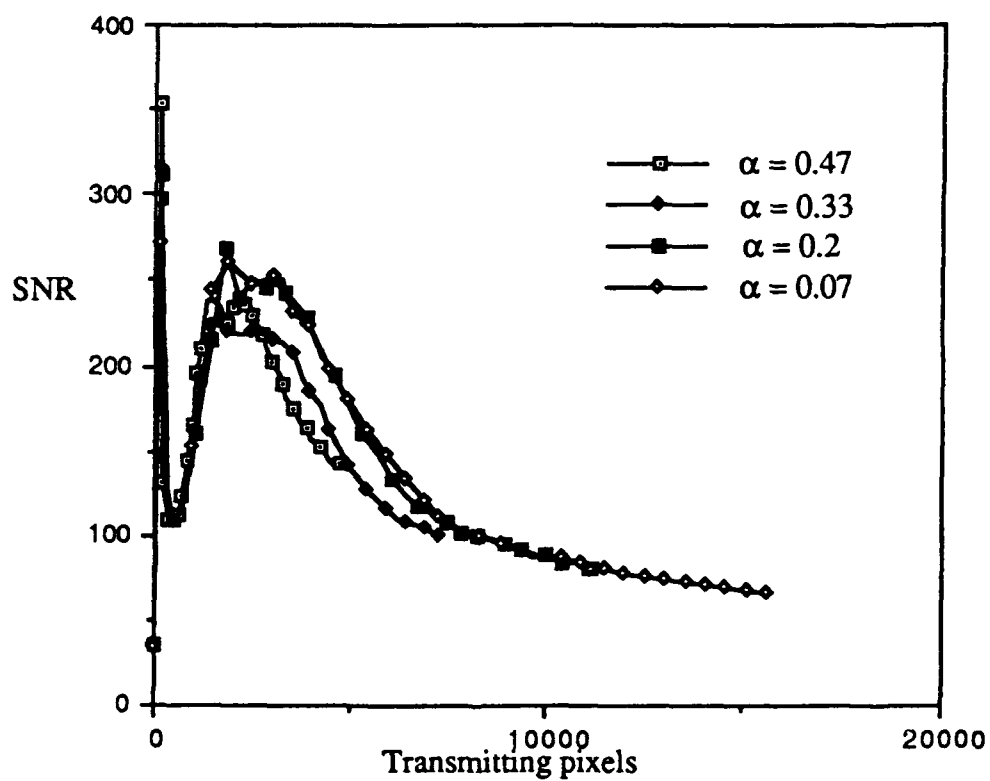
Image 28

Image 29

FIGURE 3. Examples of out-of-class images from sensor data.



(a)



(b)

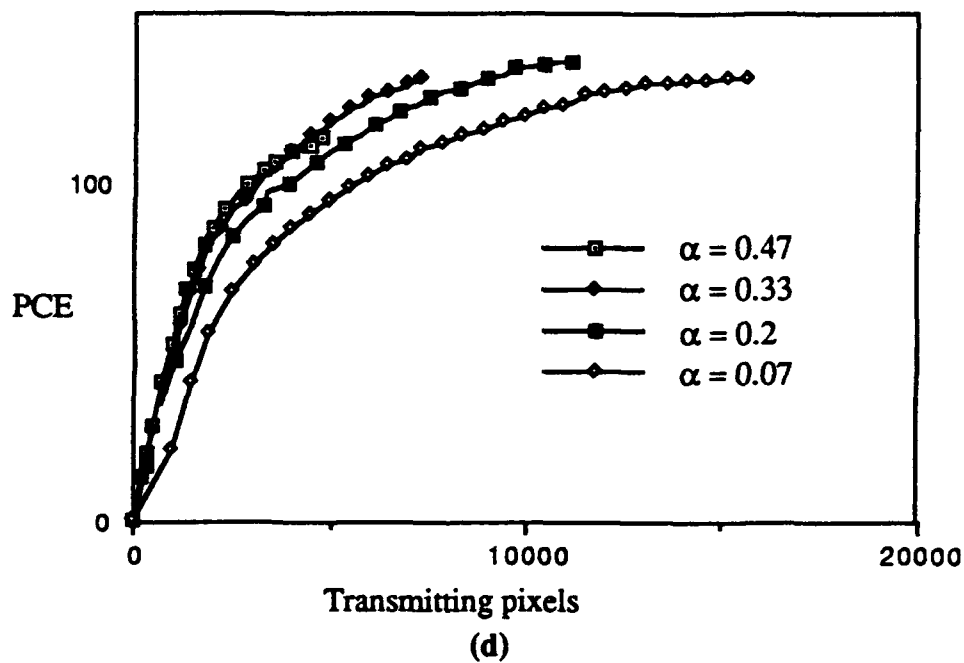
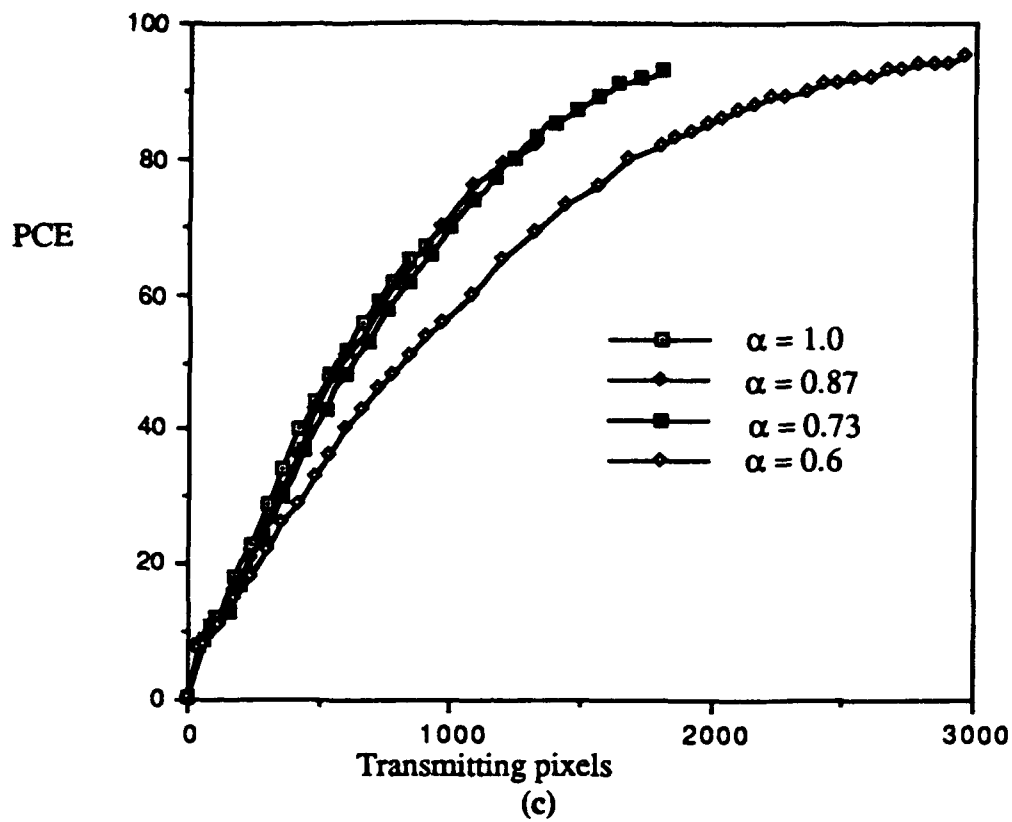


**FIGURE 4.** Graphs for different  $\alpha$  of (a), (b) SNR as a function of transmitting pixels, (c), (d) PCE as a function of transmitting pixels.

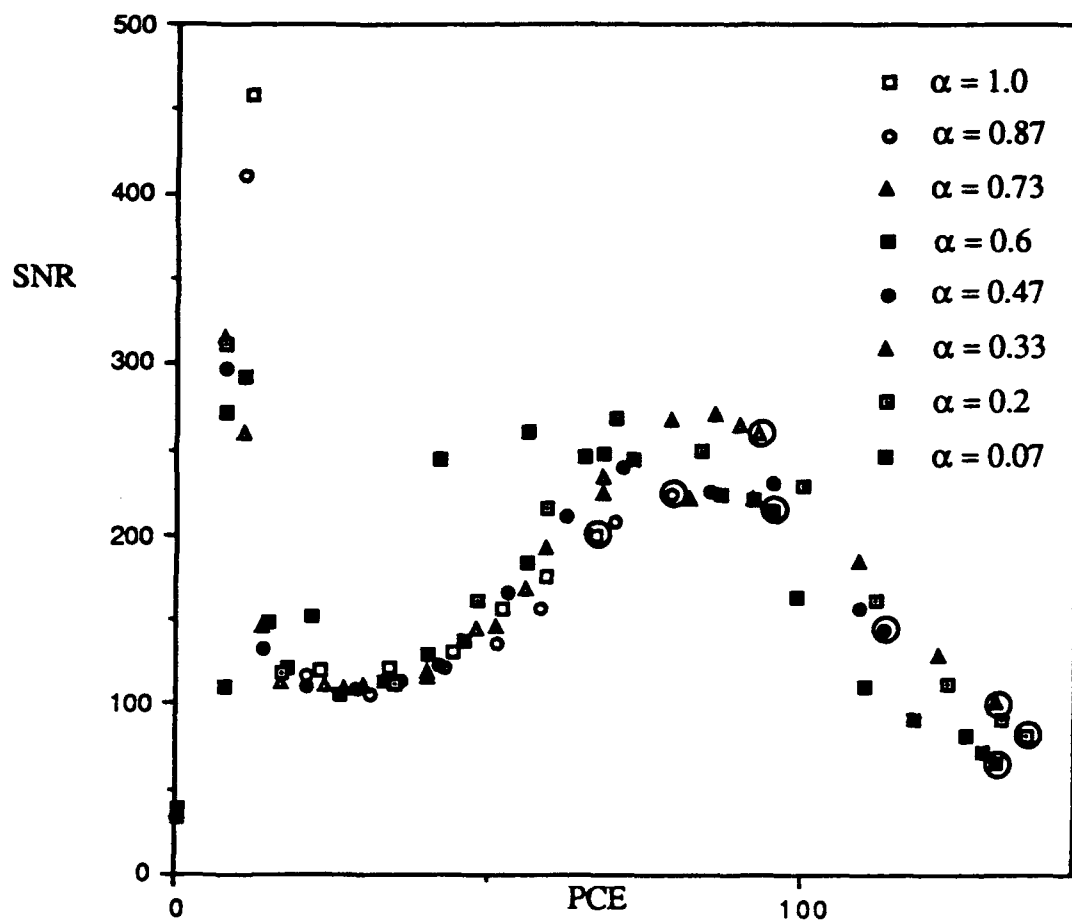


**FIGURE 5.** Scatter diagram for SNR and PCE for different  $\alpha$  using the training set.

Note that circled data points indicate filters calculated directly from Eq. (6).

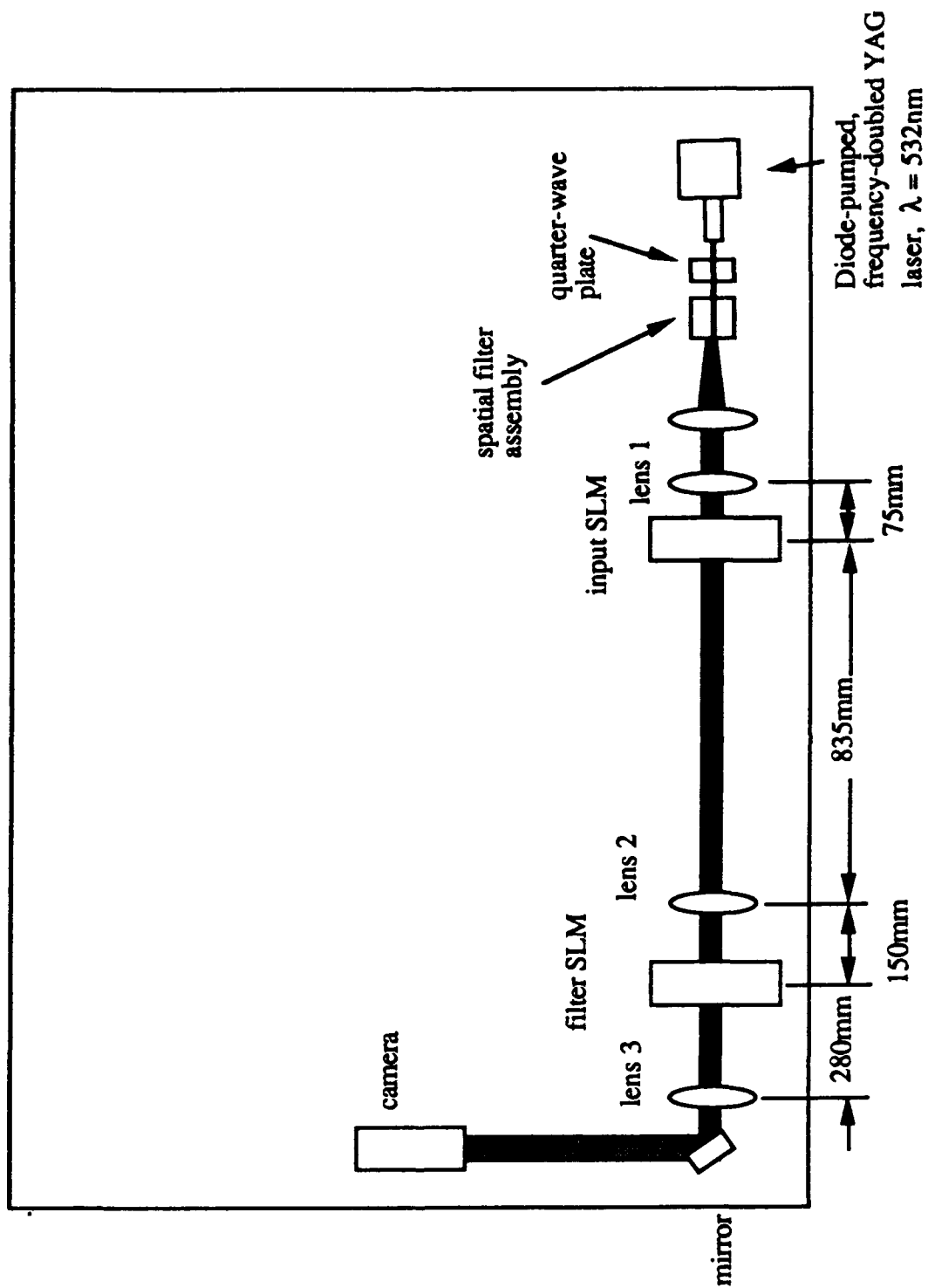


FIGURE 6. Schematic diagram of optical correlator



**MISSION**  
**OF**  
**ROME LABORATORY**

Rome Laboratory plans and executes an interdisciplinary program in research, development, test, and technology transition in support of Air Force Command, Control, Communications and Intelligence (C3I) activities for all Air Force platforms. It also executes selected acquisition programs in several areas of expertise. Technical and engineering support within areas of competence is provided to ESC Program Offices (POs) and other ESC elements to perform effective acquisition of C3I systems. In addition, Rome Laboratory's technology supports other AFMC Product Divisions, the Air Force user community, and other DOD and non-DOD agencies. Rome Laboratory maintains technical competence and research programs in areas including, but not limited to, communications, command and control, battle management, intelligence information processing, computational sciences and software producibility, wide area surveillance/sensors, signal processing, solid state sciences, photonics, electromagnetic technology, superconductivity, and electronic reliability/maintainability and testability.